PREDICTIVE LES FOR JET AEROACOUSTICS - CURRENT APPROACH AND INDUSTRIAL APPLICATION

James Tyacke[*]
Department of Engineering
University of Cambridge
Cambridge
United Kingdom
Email: jct53@cam.ac.uk

Iftekhar Naqavi
Department of Engineering
University of Cambridge
Cambridge
United Kingdom

Zhong-Nan Wang
Department of Engineering
University of Cambridge
Cambridge
United Kingdom

Paul Tucker
Department of Engineering
University of Cambridge
Cambridge
United Kingdom

Peer Boehning
Rolls-Royce Deutschland
System Design, Aeroacoustics
Dahlewitz
Germany

ABSTRACT

The major techniques for measuring jet noise have significant drawbacks, especially when including engine installation effects such as jet-flap interaction noise. Numerical methods including low order correlations and Reynolds-Averaged Navier-Stokes (RANS) are known to be deficient for complex configurations and even simple jet flows. Using high fidelity numerical methods such as Large Eddy Simulation (LES) allow conditions to be carefully controlled and quantified. LES methods are more practical and affordable than experimental campaigns. The potential to use LES methods to predict noise, identify noise risks and thus modify designs before an engine or aircraft is built is a possibility in the near future. This is particularly true for applications at lower Reynolds numbers such as jet noise of business jets and jet-flap interaction noise for under-wing engine installations. Hence, we introduce our current approaches to predicting jet noise reliably and contrast the cost of RANS-Numerical-LES (RANS-NLES) with traditional methods. Our own predictions and existing literature are used to provide a current guide, encompassing numerical aspects, meshing and acoustics processing. Other approaches are also briefly considered. We also tackle the crucial issues of how codes can be validated and verified for acoustics and how LES based methods can be introduced into industry. We consider that hybrid RANS-(N)LES is now of use to industry and contrast costs, indicating the clear advantages of eddy resolving methods.

INTRODUCTION

Aeroengine noise is a major concern for civil and military aviation industry. The European Union [1] has set the target to reduce jet engine noise by 50% from the levels of year 2000 by 2020. There are several noise sources in aero engines and jet exhaust noise, or simply jet noise, is a major contributor. In order to reduce noise, the first step is to predict noise for a given engine nozzle design. The assessment of noise from the jet engine is not just an academic exercise. There are well defined noise standards that requires measurements at three certification points (Fig. 1) given as *(a)* Approach: $2\,km$ from the runway edge under the approaching flight path, *(b)* Fly-over: $6.5\,km$ from the take-off point under the flight path and *(c)* Sideline: $450\,m$ from the runway axis during the the take-off. The noise standards demand that nozzles should be tested with an external flight stream during the design process.

---

[*]Address all correspondence to this author.

Studying a nozzle in a large open jet facility (in an anechoic chamber) has some serious drawbacks. As shown in Fig. 2, the open jet facility has a developing shear layer of the outer nozzle which can generate its own noise and sound from the main nozzle suffers diffraction from the outer shear layer. Other drawbacks include high fixed costs to maintain such facilities and relatively long turn-around times. This may be longer than 6 months to design, make and test a new configuration. Experimental tests usually allow measuring the unsteady properties in a flow at a limited number of locations (for example, using fast response probes) or only the mean flow values in a large spacial field (for example, Particle Image Velocimetry).

Numerical predictions can be a cost effective alternative to experiments, which can afford more flexibility in terms of parametric studies of various design considerations. Numerical methods benefit from the rapid increase of installed High Performance Computing (HPC) resources at constantly decreasing costs. Numerical methods can also be combined enabling multi-disciplinary optimizations. The major noise source in the jets are large scale vortical structures. It has been shown [2] that LES can resolve and predict these structures for compressible jets. The accurately predicted sound source generates noise in the near field. The linearised Euler equations can be solved numerically [3] with near field as boundary conditions to propagate the noise to the far-field [4]. However, to carry the sound to the far-field with this method requires high grid resolution, which is not a feasible option for the industrial applications. The Ffowcs Williams-Hawkings (FW-H) [5] equation or its numerical implementation, is a robust method that is often employed for far-field noise prediction.

As mentioned earlier, testing jets with a flight stream is imperative from the noise certification point of view and for (N)LES methods, introducing a flight stream is a trivial exercise as compared to experiments. The major sound sources lie within $15.0D_j$ (D_j = Jet diameter) from the engine exhaust plane. Hybrid RANS-(N)LES is an ideal candidate for noise prediction, providing accurate and reliable problem definition. The (N)LES content also reveals underlying unsteady flow and noise mechanisms. These can be investigated more deeply or isolated, in a way which cannot be achieved in an experimental test. This is in contrast to experimental facilities for which setup times are lengthy, numerous constraints exist and data sets are generally more limited. However, implementing (N)LES methods with the FW-H method for geometrically complex nozzles with various flow conditions in the engine is not a trivial exercise. It requires careful selection of numerical methods and algorithms to solve the flow equations, appropriate grid resolution for flow and near field acoustics, correct inflow and outflow boundary conditions and a judicious implementation of the FW-H method.

Although not studied here, with under-expanded jets there is a mismatch between the ambient pressure and that at the exit of the jet. This results in a series of diamond shaped shocks.

These interact with the vortical turbulent flow field and produce broadband shock associated noise (BBSAN). There is also the potential for a feedback loop with the development of the flow at the nozzle exit and the production of a screeching noise. The BBSAN makes supersonic jets noisier than subsonic. The noise impinges on the cabin and is transmitted through the fuselage and results in additional noise that passengers are subjected to. For high order, compact scheme eddy resolving simulations of this flow for both single stream and coaxial jets see [6, 7]. Notably, in this work acoustic filtering is used. With this the original near field signal is decomposed into the wavelength frequency domain and the acoustic and hydrodynamic signals are isolated. Also, spatio-temporal pressure correlations are formed based on these separate components. Using this approach both the shock cell and mixing noise components are isolated. For the use of a wavelet-based method to identify the noise signature see [8, 9] where this was shown to be effective in capturing the BBSAN aspects in both the near and far fields. Uncertainty and sensitivity analysis are also performed in [10] indicating local sensitivity within the shock cell feedback loop, requiring deeper analysis using LES and DNS.

Gand [11] contrasts Delayed-Detached Eddy Simulation (DDES), Zonal Detached Eddy Simulation (ZDES) and ZDES with additional synthetic turbulence. The initial shear layer transition is delayed using DDES unless a filter width based on local vorticity is used with shielding functions near walls. Similar filter modifications are made by Shur et al. [12]. Gand shows synthetic turbulence based on a typical grid generated turbulence length scale at various intensities can improve shear layer development and speed up transition. However, in many cases the strict zonalisation used does not delay transition nor utilises synthetic turbulence and provides similar results. Brunet [13] also introduces isotropic turbulence in an installed coaxial nozzle. Overall agreement with measurements is improved, particularly mean axial velocity alignment with shock cells. However, in a real engine, turbulence will have significantly different scale and structure both at walls and in the obstructed core and bypass streams. Bres et al. [14] use synthetic turbulence, local grid refinement and wall modelling inside a jet nozzle to replicate the experiments conditions. Mesh refinement int he nozzle and wall modelling were found to be most important. Cetin et al (2016) [15] introduce a centre body and struts in a jet nozzle achieving agreement with experiments. The centre body and struts generated a peak in velocity spectra at $St = 0.15$ and a reduction in turbulent length scales at the nozzle exit respectively. As noted by Verriere [16] shear layer development is difficult to accurately capture especially with low velocity ratios often found in modern coaxial nozzles. This is demonstrated by Tyacke et al. [17] for a hot jet which tends to relaminarise. Using body forces, fan, guide vanes, A-frames and a gearbox shaft are added to the bypass duct yielding more rapid inner shear layer development. Verrierre also makes use of a wiggle detector to
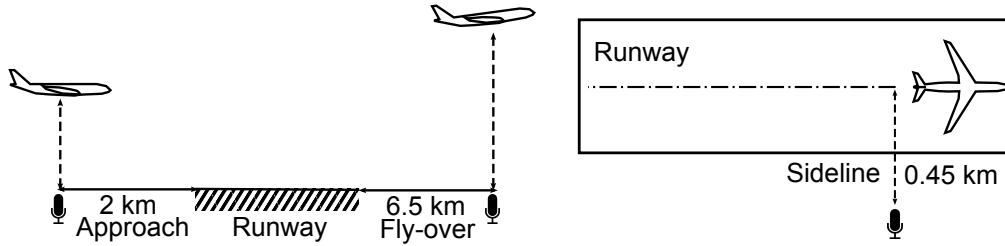
FIGURE 1. Definition of certification points for the noise measurement: Approach, fly-over and sideline.
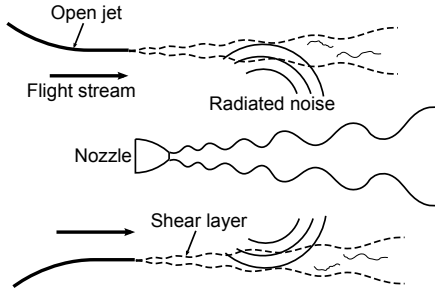

FIGURE 2. Open jet facility to measure jet noise with a flight stream.

dynamically apply only a minimal level of numerical dissipation to stabilise the solution. Vogel et al. [18] use LES and a numerical source localisation array to identify frequency changes due to installation effects. They find an increase of low frequency noise near the wing trailing edge and a reduction of high frequency noise normally associated with the nozzle lip region due to shielding. Using the FWH method, Rahier et al. [19] introduce additional flux terms providing a deeper understanding of spurious noise generated at the FWH end disc by vortical structures. Terms to approximate the usually neglected volume integral at the end disc are evaluated. A closed surface with these additional terms was most advantageous for a jet and may in future be a useful approach for complex geometries or those with a flight stream. Lyubimov [20] applies hybrid RANS-NLES to study jet nozzles including three with chevrons. Using a 9th order instead of a 5th order Weighted Essentially Non-Oscillatory (WENO) scheme improves flow prediction on the modest grids used (circa 2.5 million cells). A backward facing step is introduced to generate inlet turbulence, the dimensions of which could have significant impact on results. High frequency pressure waves are formed on the lobes of the jet, the intensity of which is proportional to the lobe length. Rosa et al. [21] study flow anisotropy and length scale effects in hot and cold jets based on LES data. Time and length scales increase in the hot jet. LES data is utilised to indicate improvements to RANS modelling and hence far field predictions using the Lighthill Acoustic Analogy. LES and RANS are used in [22] extending the achievable frequency range that can be predicted. Various previous acoustic modelling approximations are shown to be incorrect using the

LES data. Similar work is extended to chevron nozzles and the use of micro-jets in [23]. Effects of chevron penetration angle, number and micro-jet mass flow rate are studied revealing critical values where noise reduction benefits decline relative to loss of thrust. Towne et al. [24] characterise and model waves that can be trapped within the potential core of subsonic jets. They compare their acoustic modelling with LES data showing good agreement. The model reveals resonant frequency bands that exist only under certain Mach numbers and temperature ratios.

Many past studies have focused efforts on LES of low Reynolds number single stream cold or hot jets. As demonstrated, LES now has a wide range of application in acoustic prediction, sound source localisation and the improvement of lower order models.

In this paper a framework is presented to perform hybrid RANS-NLES for complex geometry nozzles with the implementation of FW-H method to predict the far-field noise accurately. The techniques and methods discussed here are based on the authors' experience with a well developed and extensively tested code HYDRA [25]. This code has been used to study single stream nozzles with and without flight stream [26, 27], chevron nozzles [28] and nozzles with installation effects [17]. These previous studies have provided the guidelines for the key aspects including grid resolution for various jets, numerical techniques, data acquisition and implementation of the FW-H method for far-field noise prediction.

In this work numerical schemes and boundary conditions will be described, which have been tested for various jet flows. Meshing requirements will be discussed before the acoustic methods used to predict far field noise. Alternative methods are also considered. The future use of LES methods for jet noise prediction in industry is also discussed with quality assurance and costs considered before conclusions are drawn.

NUMERICAL MODELLING
Turbulence Treatment

As noted, jet flows are well suited to eddy resolving methods due to the formation of free shear layers and large unsteady coherent structures. In the current method, these large structures fall into the wake type flow category as outlined in [29, 30]
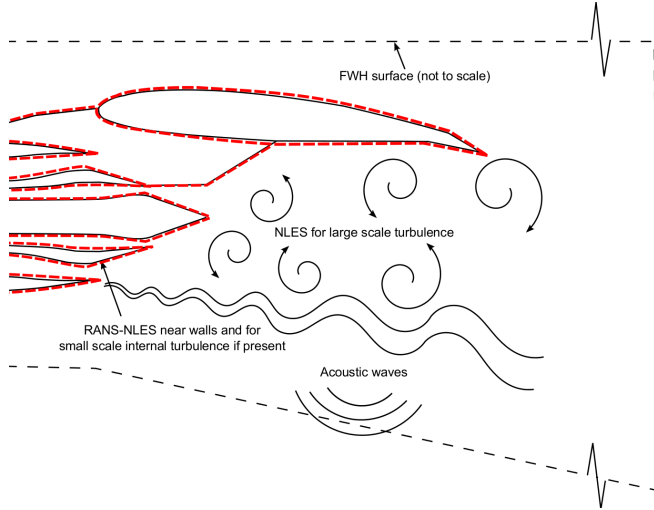
FIGURE 3. Flow features and turbulence modelling approach.

and are resolved using NLES. NLES uses no explicit subgrid scale model, instead using numerical dissipation to drain energy. The smaller scales near the nozzle are also resolved using NLES hence the mesh is refined in these regions. Near walls, to reduce the high (N)LES grid requirements typically needed to resolve fine streak structures, a RANS layer is used to model this region, allowing a larger mesh spacing to be used. This is indicated in Fig. 3. This layer is used for the inner boundary layer and blended to a NLES region using a Hamlton-Jacobi equation: $|\nabla \tilde{d}| = 1 + f(\tilde{d})\nabla^2 \tilde{d} + g(d)$. This modifies the true wall distance in the Spalart-Allmaras RANS model [31], retaining RANS behaviour in the inner layer and reducing the eddy viscosity to zero in the NLES region. Further details can be found in [32]. The heated jet KEP results presented use an explicit Smagorinsky model [33] outside the RANS layer and lower numerical dissipation instead of NLES, both strategies giving valid results.

Numercial Discretisations

Since around 90 percent of the flow energy should be resolved in (N)LES instead of modeled in RANS, the numerical methods are much more demanding in the LES context. The LES subgrid stress (SGS) viscosity used is much less than the eddy viscosity in RANS models, so excessive numerical dissipation overwhelms the SGS viscosity and eradicates the turbulent eddies that should be resolved in LES. It will eventually deteriorate the simulation accuracy and fidelity. Generally speaking, LES requires the numerical dissipation to be at least lower than the SGS viscosity if an explicit SGS model is used in the simulation. A low-dissipation numerical scheme is hence preferable for eddy resolving simulations, such as (N)LES and DNS.

Numerical dissipation is commonly used to suppress numerical instabilities. The reduction of numerical dissipation can

make traditional numerical schemes unstable. To overcome this problem, the kinetic energy preserving (KEP) is used in our code to stabilize the computation without any numerical viscosity [27, 34]. From a physical point of view, the KEP is one of the crucial elements in the turbulence cascade process, where energy is transferred among different flow scales. The KEP scheme is a type of central scheme based on the skew operator [35]. The KEP scheme is used to replace the central part of the Roe scheme but the fourth order smoothing terms are retained to be active in the sponge region where very coarse grids are used to damp the flow and acoustic waves away from the region of interest. This also prevents any reflection from the boundaries. More details about the sponge region are to be discussed in the next section. This overall methodology is used and well validated in the earlier works of jet noise simulation [27, 28]. The low-dissipation discretization takes the form of

$$F_n^I = F_n^{KEP} - \frac{1}{2}\varepsilon |A_n| \left[L(U_R) - L(U_L)\right] \tag{1}$$

where

$$F_n^{KEP} = \begin{bmatrix} \overline{\rho \overline{u_n}} \\ \overline{\rho \overline{u_n}\vec{\overline{u}} + \overline{p}\vec{n}} \\ \overline{\rho \overline{u_n}\overline{H}} \end{bmatrix} \tag{2}$$

F_n is the surface normal flux vector, U is the conservative variable vector, $|A_n| = (\partial F/\partial U)_n$ is absolute Jacobian matrix, L is the pseudo Laplacian operator, and the over bar $\overline{()}$ is the averaging operator on two nodes of the edge, the subscript L and R is the right and left nodes on an edge across the control volume surface. The parameter ε controls artificial dissipation in the simulation. In the (N)LES zone, ε is kept at a low level and is increased to develop the sponge region near the boundary.

A series of validation cases have been carried out on canonical flows to show the suitability of KEP for eddy resolving simulations. For example, the computation of the Tollmien-Schlichting (T-S) instability wave and homogeneous isotropic decaying turbulence (HIDT) are illustrated in Fig. 4 by comparing with the second order upwind Roe scheme. Generally, the KEP is less dissipative and more accurate than the conventional Roe scheme. It can better predict the T-S instability wave development in the channel with less artificial damping. The KEP shows great advantages over the upwinding scheme in the HIDT case, accurately predicting the energy transferring in the high wave number range of the isotropic turbulence, which is crucial to high fidelity eddy resolving simulations. The KEP's insensitivty to cell type displayed in Fig. 4(b) has allowed the use of hybrid structured-unstructured mesh generation as shown later.
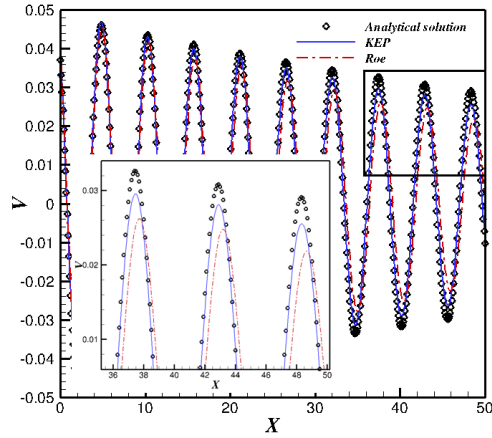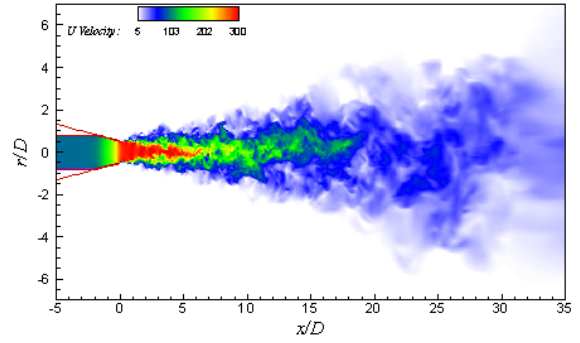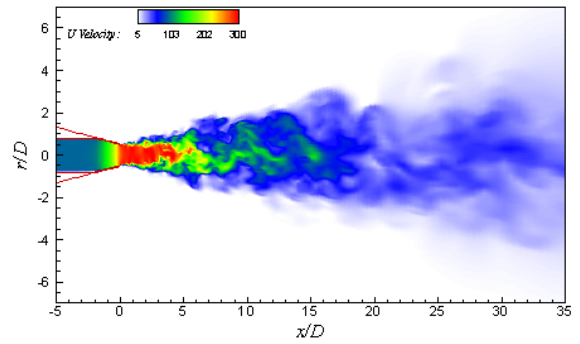
(a) Tollmien-Schlichting Wave
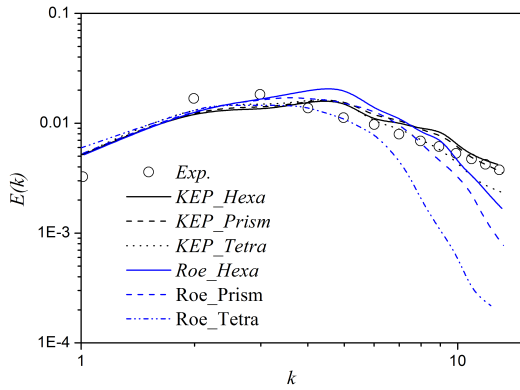
(b) Homogeneous Isotropic Decaying Turbulence

FIGURE 4.   Validation of KEP scheme on the canonical flow cases.

(a) KEP scheme

(b) Roe scheme

FIGURE 5.   The axial velocity field of a subsonic jet simulated by KEP scheme and Roe scheme.

For practical jet prediction, the low-dissipation KEP advantage is demonstrated in a subsonic hot jet simulation. RANS-(N)LES of jets with far-field sound predictions have been carried out by Wang et al. [27] using the KEP scheme. The results showed encouraging agreement with measurements. A contrast is made for heated jets here with the upwinding Roe scheme, shown in Fig. 5. It is found that much smaller turbulent structures can be supported in the KEP simulation than that in the Roe schemes result. Figure 6 shows the quantitative comparison that the potential core length and the shear layer development are better predicted by the KEP scheme, better agreement with the measurements especially in terms of the turbulence fluctuation. The dissipative upwind scheme distorts the turbulence intensity along the centerline and damps it much faster along the lipline. However, the KEP is not perfect. It actually struggles and exhibits dispersive oscillations instead of dissipating the unresolved energy when the grid is coarse in the high gradient region. Therefore, it

indicates that the grid needs to be refined in that region or dissipation added to suppress the dispersion. When the Mach number is high, especially when a shock wave is present, the KEP needs an extremely large number of cells to resolve the discontinuity, as Jameson estimated [35]. To capture the shock on relatively coarse grids, the KEP could be used with carefully tuned artificial bulk diffusivity [36] or by blending with upwind scheme [37] in (N)LES based computations. This upwinding would be in the locality of the shock and minimised to have negligible impact on the turbulence. In our experience, the KEP scheme is an encouraging choice to perform hybrid RANS-(N)LES on complex geometry jets with unstructured meshes.

Nonreflective Numerical Boundary Treatments

Aeroacoustic predictions are sensitive to reflections at the numerical boundary. To prevent this boundary reflection, a numerical sponge zone is placed near the computational boundary to dissipate the outflowing structures and absorb any reflections. Here, the sponge zone is achieved by increasing the parameter ε in equation (1) from the (N)LES zone edge to the numerical boundary, shown in Fig. 7. The high order numerical dissipation is fully active in the sponge zone with a blending from the
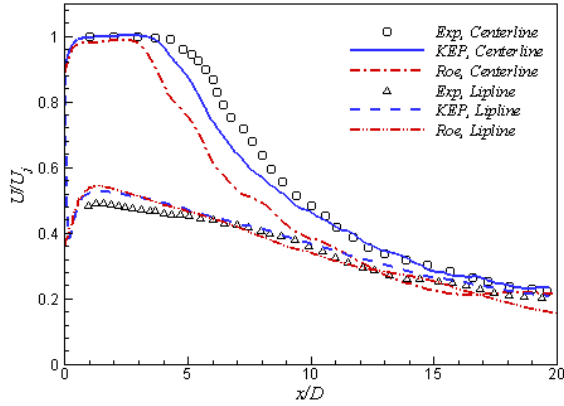
(a) Axial Velocity
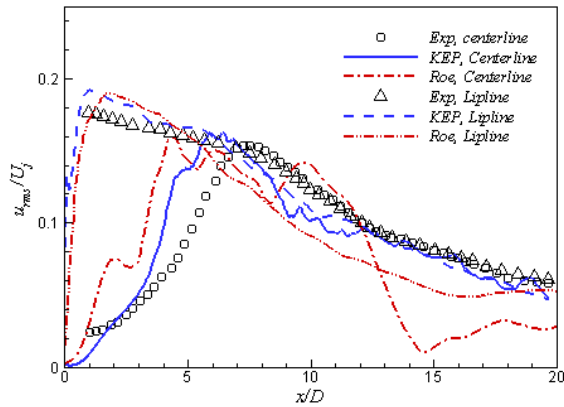
(b) Turbulence Intensity

FIGURE 6. Axial velocity and turbulence intensity along the center-line and nozzle lipline.

FIGURE 7. Numerical boundary treatment illustration.

(N)LES region, where a low level of numerical smoothing suppresses dispersion. This maintains accuracy in the key flow and acoustics region. The increasing dissipation is also in conjunction with the grid stretching towards the boundary, which creates the sponge zone at minimal computational cost. The sponge region is determined with previous experience and improved by assessing initial data. The boundaries are placed sufficiently far away, that no boundary reflections have been detected. There are a range of other non-reflective boundary approaches [38–40], however these are not outlined here.

Inflow

Many studies have focused on the development of jets after the nozzle exit. The upstream boundary layer has also been shown to affect shear layer development, particularly the relation between azimuthal and axial structures, peak turbulence intensity and spreading rate for round [41] and chevron nozzles [42]. Bodoney et al. also present an overview of literature [2] describ-
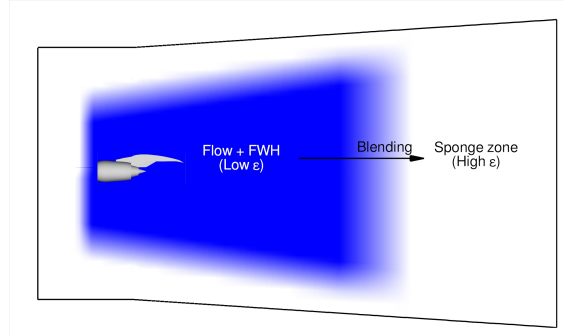
ing the influence of shear layer thickness and inflow forcing. Uzun and Hussaini [42] and Birch [43] note the importance of running simulations over a critical Reynolds number of 0.5 million and with turbulent thin initial shear layers so that far field noise predictions become independent of *Re*. This can become computationally expensive, however locally, overset and unstructured mesh approaches can minimise these additional costs. To introduce the effect of upstream turbulence with reduced mesh size, a wide range of synthetic turbulence methods have been developed [44–47]. The most commonly used are those based on Lund's recycling [48], introducing boundary layer turbulence near the nozzle exit and avoiding upstream mesh cost. In real engines however, the upstream boundary layer is also influenced by all upstream features including large scale geometry and complex flow and acoustic interactions. Tyacke et al. [17] use body force modelling to introduce bypass duct turbulence from the fan, guide vanes, A-frame supports and gear box shaft. The effect of this upstream turbulence is shown to move the inner shear layer transition point upstream. Hence, for real engine applications, additional upstream effects can be modelled for additional accuracy, however the effect is secondary compared to other influences such as discretisation and FWH surface placement and processing. Care must be taken not to artifically transition the shear layers via upstream disturbances, particularly with coaxial hot jets there the inner shear layer is weak and can re-laminarise downstream of the nozzle exit. The high Reynolds numbers involved currently necessitate the use of lower order modelling, to produce meaningful flow conditions at the nozzle exit. There are clearly different inflow requirements to model experiments or true engine conditions.

MESH GENERATION

A high quality mesh is imperative to successful acoustics simulations. Cell type, quality and distribution all play a crucial role. For many current second order solvers, hexahedral cells are preferred to reduce numerical dissipation [49, 50]. A key aspect is to ensure the mesh follows the shear layers and expands
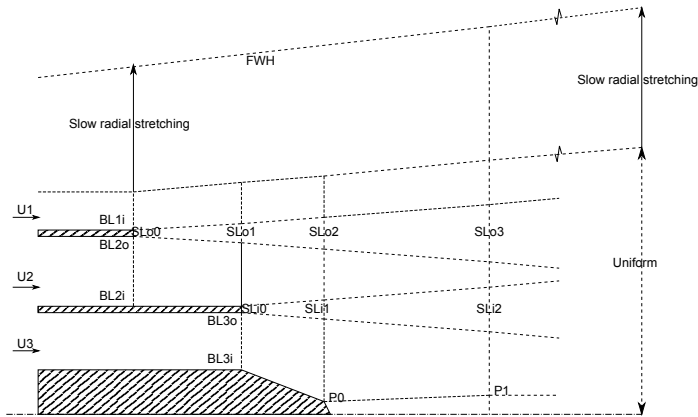
FIGURE 8. Typical round nozzle mesh topology.

slowly in the radial and axial directions. A geometric expansion ratio of approximately 1% [51] is recommended in the axial and radial directions. A more rapid axial expansion corrupts the accurate resolution of the convecting turbulent structures responsible for noise generation, creating spurious sound sources in the flow. Radially, the frequencies of interest at the FWH surfaces limit the mesh spacing, following a Strouhal number limit of $St_{max} = D/(8M_a\Delta R)$ [50]. Within the jet plume, the radial spacing becomes uniform between $2.5 < x/D < 5$, near the end of the potential core. Figure 8 shows a typical structured mesh blocking topology for a coaxial jet with a central plug in the $x-R$ plane. Indicated are three fluid streams $U1, U2, U3$ representing the flight stream, bypass and core flows for an engine respectively. Boundary layers for each fluid stream are indicated by $BL1, BL2, BL3$ with i and o indicating inner and outer radial locations. The plug, inner and outer shear layers are indicated by P, SLi, SLo with numbers indicating the axial location index. For a round single stream nozzle, only $U1$ and $U2$ require consideration. Each fluid stream may have a different velocity, density and temperature. The nozzle geometry and wide range of parameters affecting shear layer development make the location of the block vertices and mesh distribution difficult to determine *a priori*, particularly for coaxial nozzles. Even for single stream nozzles, the nozzle design can have a strong impact on the mean and turbulent flow structure. For example there is usually strong acceleration near the nozzle exit. It has also been shown that large scale upstream turbulence from the engine can expedite shear layer transition, moving it upstream [17]. RANS may be used to provide estimates of initial shear layer thickness and trajectories. Although RANS is known to be generally unreliable for free shear flows and is often insensitive to several turbulence phenomena, a two-equation model may be adequate to provide guidance for preliminary runs. After this, small adjustments may be made based on the initial developed (N)LES flow to improve resolution and quality. Preferably this would be achieved in an

automated fashion using flow gradients or error estimates such as adjoint methods.

For the internal boundary layers, a mesh adequate for the turbulence modelling employed is sufficient using local y^+ values to ensure the mesh is not over-refined near the walls. In the boundary layers, the number of wall normal nodes lie in the range of 20-30 [41]. The boundary layer mesh can put significant restrictions on the CFL number near the lip, particularly for flows generating high shear or for blunt lip edges. This is because the initial radial velocity fluctuations can become high, passing through thin cells. Near the lip, a more rapid radial expansion is acceptable to alleviate this issue, whilst still providing approximately 10 cells across each integral length scale [41]. This can significantly increase the time step achievable.

Table 1 indicates a summary of mesh resolution at different locations in Fig. 8 for recent cases at $2 \times 10^5 < Re < 4 \times 10^5$. These are an indication of our current experience and are in accord with other recent literature [50, 52], as shown by Fig. 9. Around 66% of the mesh lies in the acoustic region between the jet plume and the FWH surfaces. This indicates that higher order methods that efficiently propagate pressure waves may provide significant computational savings. Only 7% lies in the sponge region outside of these zones, indicating only a small gain might be achieved from smaller domains with non-reflecting boundary conditions. For cases with a flight stream which elongates the jet plume reducing it's radial extent, around 5% of mesh is transferred from the radial direction to be placed further downstream in the axial direction. Care must be taken with cell aspect ratio which can reach orders in excess of 100, hence filter definition, discretisation and turbulence modelling must be synergistic.

Azimuthal resolution

The azimuthal resolution can be an important factor in a successful time-resolved jet simulation. Not only does it limit the resolved frequency range (although most acoustic waves predominantly propagate radially), it is also necessary to adequately resolve the flow structure near the nozzle. Table 2 shows typical azimuthal resolution for our RANS-NLES based approach, which is contrasted with other literature. Resolving inlet or boundary layer turbulence requires a significantly higher number of nodes. For RANS-NLES, near wall turbulence is modelled, relieving mesh requirements. Larger scale turbulence from upstream will require adequate mesh to resolve the dominant structures.

To reduce the cost of eddy resolving methods, it may be necessary to use different azimuthal resolution in different regions of the flow. For this purpose, overset meshes [17] or hybrid structured-unstructured meshes [53] seem promising. Figure 10(a) shows a fully structured mesh in an axial plane of a coaxial nozzle with 160 azimuthal cells. Figure 10(b) shows a hybrid structured-unstructured mesh with 40, 80 and 160 azimuthal cells at the plug, inner and outer shear layers respec-

TABLE 1. Typical vertex locations and number of mesh spacings per notional outer jet diameter in relation to Figure 8. Numbers in brackets refer to single stream cases.

	P0	P1	P2	P3	SLi0	SLi1	SLi2	SLi3	SLi4
x/D	0.87	2.13	4.75	10.00	0.31	0.87	2.13	4.75	10.00
R/D	0.00	0.02	0.07	0.18	0.26	0.17	0.18	0.29	0.52
$D/\Delta x$	163	115	63	32	230	171	110	65	31
$D/\Delta R$	34520	1704	377	168	49331	5391	926	237	175

	SLo0	SLo1	SLo2	SLo3	SLo4	SLo5	FWH
x/D	0.00 (0.00)	0.31 (-)	0.87 (0.98)	2.13 (1.97)	4.75 (4.92)	10.00 (9.84)	(all)
R/D	0.50 (0.50)	0.45 (-)	0.40 (0.50)	0.47 (0.50)	0.65 (0.67)	0.99 (0.94)	7.5
$D/\Delta x$	235 (156)	235 (-)	172 (135)	109 (114)	65 (74)	31 (54)	$\approx \Delta x_{SL_o}$
$D/\Delta R$	49331 (20320)	14694 (-)	2009 (1016)	384 (508)	203 (254)	173 (102)	10 (8)

TABLE 2. Azimuthal resolution of current simulations and those in literature.

Case	Current	Bodony 2008	Mendez 2012	Bres 2012	Bres 2011	Bogey 2012
N_θ	140-200 (RANS-NLES)	32-208 (collated)	128 (laminar BL)	160 (laminar BL)	16-512 (locally refined)	1024 (BL resolving)

tively. The difference in cell count is 20% and the unstructured mesh lies in the benign zone between two high quality hexahedral meshes which resolve the shear layers. In the axial direction, where the shear layers eventually meet (radially), axial unstructured elements will be required to reconcile the two resolutions into a lower azimuthal resolution. This would further reduce mesh size. Ideally this resolution change would be done gradually with non-hexahedral elements interspersed throughout the mesh. However, unstructured anisotropic hexahedral dominant meshes are still a topic of active research. For internal turbulence, a high azimuthal resolution would be required inside the nozzle and for a short development region downstream, hence the figures provided are for demonstrative purposes only.

Unresolved issues

Installed configurations   More complex configurations are a challenge to tackle even to generate a preliminary mesh. The introduction of a wing, flap and pylon into a structured mesh creates a number of undesirable blocks. Using structured meshes, clustering of the mesh near the pylon sidewalls propagates radially throughout the nozzle, requiring careful redistribution. Non two-dimensional wing sections also cause structured meshes to become squeezed or stretched at the wing tip and root. A separate wing and flap configuration to include flap noise effects also introduces significant mesh clustering and additional blocks. Especially problematic regions are those where two surfaces meet at an acute angle forming a thin, sliver gap, such as the junction at either end of a realistic flap-wing. These aspects can lead to rapid cell expansion, high skewness and poor mesh

quality as attempts are made to reconcile different local mesh zone requirements. In the region between the nozzle and wing, there is a need to have a grid resolution that adequately adheres to boundary layer requirements on the wing, whilst also respecting the spacing requirements of the jet free shear layers. The proximity of the nozzle to the wing continues to reduce as bypass ratios increase leaving little room for blending of mesh regions. In our limited experience, the axial mesh distribution of the wing and free shear layers is similar.

Figure 11(a) shows a hybrid meshing strategy for a round nozzle. Hybrid meshes seem well suited to tackling complex configurations, where a high quality hexahedral mesh is used for the jet plume, whilst unstructured mesh is used for complex geometry and is interfaced where cell aspect ratios are similar to avoid cell volume jumps. As shown in Fig. 11(b), this can be extended to installed cases where complex wing and flap mesh uses unstructured surface mesh layers to generate hexahedral cells interfaced with unstructured isotopic elements.

Lower order modelling of some geometry allows more complex configurations to be tackled at lower cost. Figure 12 shows an installed jet with body force modelling of internal geometry, leading to accelerated shear layer development. Installed Ultra High Bypass Ratio engines and chevron nozzles designed to lower noise, can compound problems with mesh blocking and distribution. As shown in Fig. 13(a), unstructured hexahedral (Octree-type) meshes have become popular for tackling complex geometry, however, they are unsuitable for acoustics. The rapid cell expansion puts a limit on Strouhal number or generates high cell counts and introduces discontinuities in the (N)LES filter
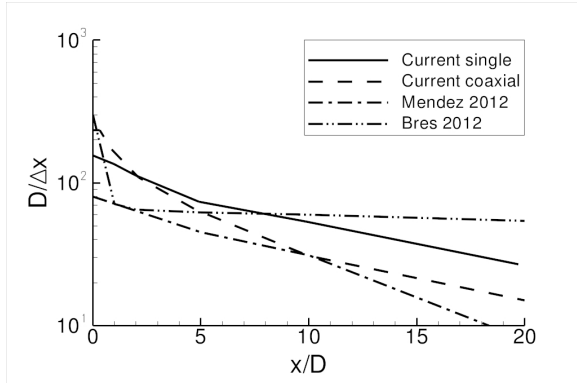
(a) Axial
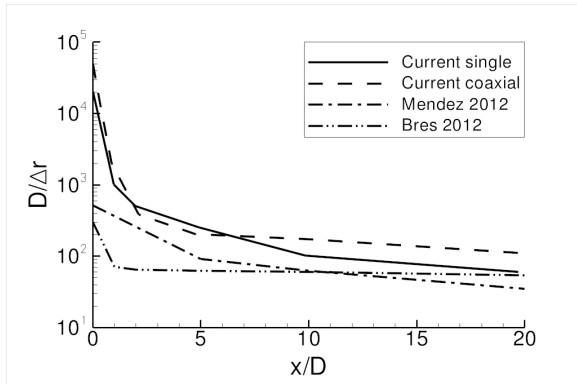
(b) Radial

FIGURE 9. Comparison of current axial and radial mesh spacings with other literature. I.e. number of spacings per notional jet diameter along SLo.
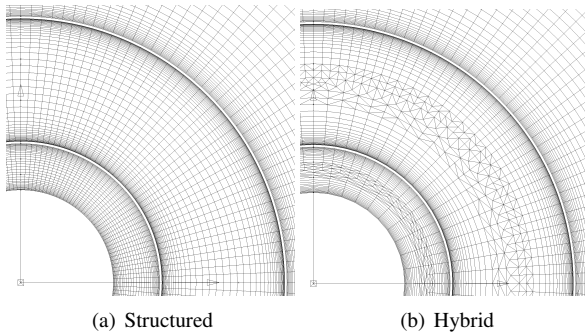
(a) Structured   (b) Hybrid

FIGURE 10. Structured and hybrid axial mesh planes showing azimuthal mesh structure.

width. However, they can be used in conjunction with RANS to inform meshing, for example, the non-axisymmetric distortion of the shear layers by a wing as shown in Fig. 13(b). After this, an improved (N)LES or hybrid RANS-(N)LES mesh can be generated.
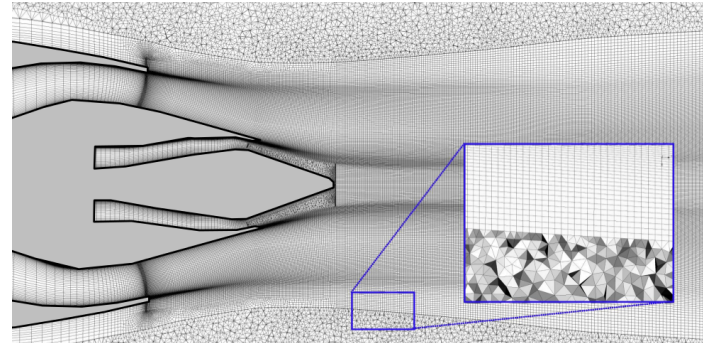
(a) Round nozzle
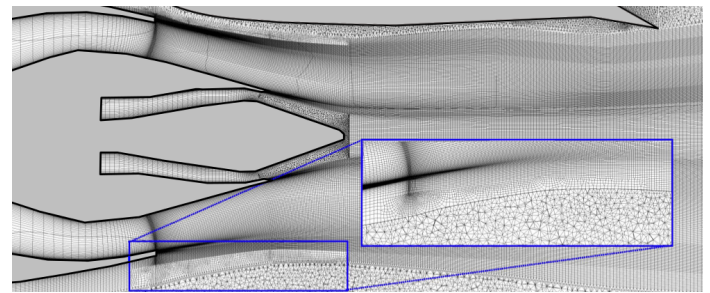
(b) Installed round nozzle

FIGURE 11. Hybrid structured-unstructured mesh for (a), an isolated nozzle with the inset showing the structured-unstructured interface and (b), an initial installed round coaxial nozzle with an inset showing regions of different axial resolution.
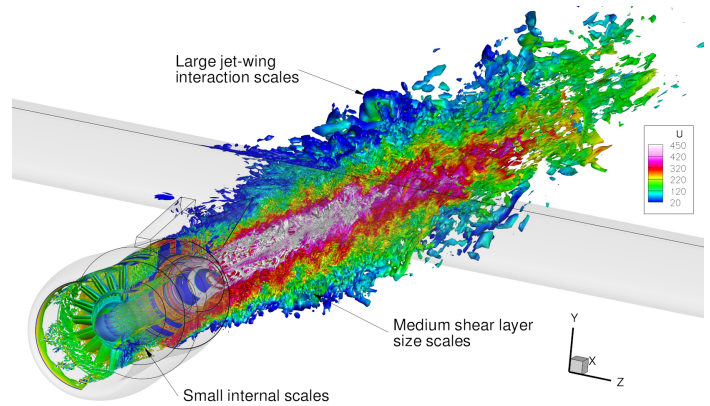
FIGURE 12. RANS-NLES of an installed engine with internal geometry modelling.

Chevron nozzles To reduce perceived noise, chevron nozzles have been identified as having potential. Generally, more aggressive single stream nozzles with large chevrons have been studied [28, 54]. For commercial flights a larger number of less aggressive chevrons are more viable options, targeting noise reduction in specific frequency ranges whilst balancing specific
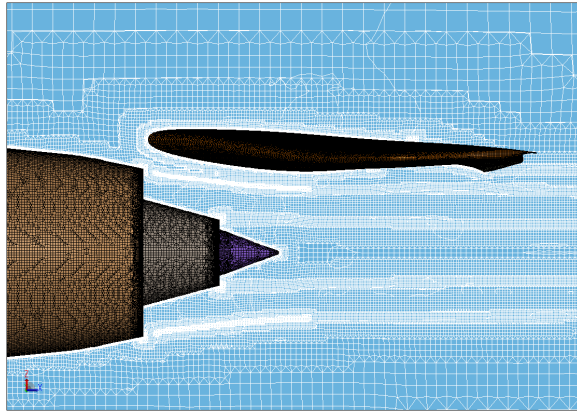
(a)
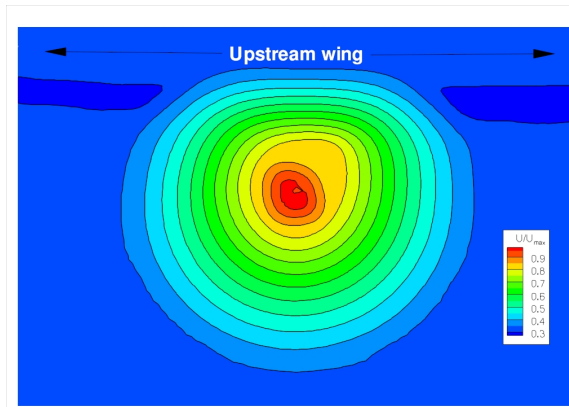
(b)

FIGURE 13.   (a) Unstructured hexahedral Octree mesh of an installed nozzle, (b) axial velocity contours at $x/D = 3$ ($1D$ downstream of the wing trailing edge).

fuel consumption penalties. With engine diameter increasing and becoming closer to the wing, part-annulus chevron configurations have also been considered. Other key parameters include, sharp or blunt chevrons, penetration angle and chevron depth. Clearly, these heavily influence mesh design and distribution, and relatively few configurations have been tested experimentally or using CFD, particularly for coaxial nozzles. Hence, although chevrons pose an unresolved issue, we attempt to provide some guidance based on our current knowledge and practice.

For round nozzles, the shear layers usually approximately follow the angle of the nozzle exit at the lip for the first mesh block. For chevron nozzles, this is not the case and radial variations of the mesh are required azimuthally [28]. Flow gradients and velocity ratios have previously been used successfully to move mesh to follow the complex shear layers [42]. It may be possible to use similar automated methods after the best initial mesh has been generated. Again RANS may be used for guid-

ance near the nozzle with the mesh rapidly expanding to a more uniform state within approximately $2D$ [28, 54]. Within a hybrid mesh, chevrons can be introduced by replacing a structured mesh region near the nozzle with unstructured mesh. Such a topology is shown in Fig. 14(a). An example mesh in the chevron region is enlarged in Fig. 14(b). Using advancing front, quadrilateral dominant unstructured patches, mostly hexahedral elements can be generated from boundaries around the chevron and interfaced with the surrounding structured mesh using tetrahedra when the cell aspect ratio matches that of the surrounding mesh. This approach also allows local azimuthal refinement, to resolve higher azimuthal modes [54]. For specified configurations, zonalised hybrid meshing could be an automated process and may be useful in interfacing meshes for nozzles and wings for installed cases. Hessian matrix based mesh movement and grid adaptation are envisioned as tools to improve complex mesh distributions.

FFOWCS WILLIAMS-HAWKINGS METHOD FOR FAR-FIELD NOISE PREDICTION

There exists a range of methods to convert near field sound source data to far field sound. These include chiefly, Kirchoff and FW-H surface methods. Here we focus on FW-H but both have similar limitations, typically having surface location sensitivity. The original form of the FW-H equation involves a volume integral term, which is very expensive to calculate. However, it is negligibly small when all noise sources lie within an enclosed, permeable FW-H surface and is hence ignored. The resulting far-field pressure fluctuations p' are calculated from surface integrals.

An important aspect of the FW-H method is the selection of the FW-H surface position, where unsteady data is stored and the surface integrals are evaluated. There is no consensus among the jet aeroacoustic community on the shape and position of the FW-H surface. The FW-H surfaces have been placed close to the shear layer [55] as well as away from the jet [42]. Generally, for round jets the FW-H surface is an axi-symmetric conical or cylindrical surface around the jet. In the absence of the volume integral, the FW-H surface should encompass all the sound sources in the jet. The FW-H surfaces have closing-discs at both ends, as shown in Figure 15, to achieve this objective.

It has been shown [51, 56] that the FW-H surfaces just at the outer edges of the shear layer give spurious noise at low frequencies. The spurious noise is associated with the hydrodynamic disturbances of the flow rather than the acoustic signal. Similarly, when the closing disc is placed at the downstream end of the FW-H surface, it also suffers from the passing vortical structures and generates spurious hydrodynamic noise. In order to eliminate spurious hydrodynamic noise from the closing disc multiple closing discs are used as shown in Fig. 15. The far-field pressure fluctuations are calculated with each closing disc individually and the resulting time series are averaged to eliminate
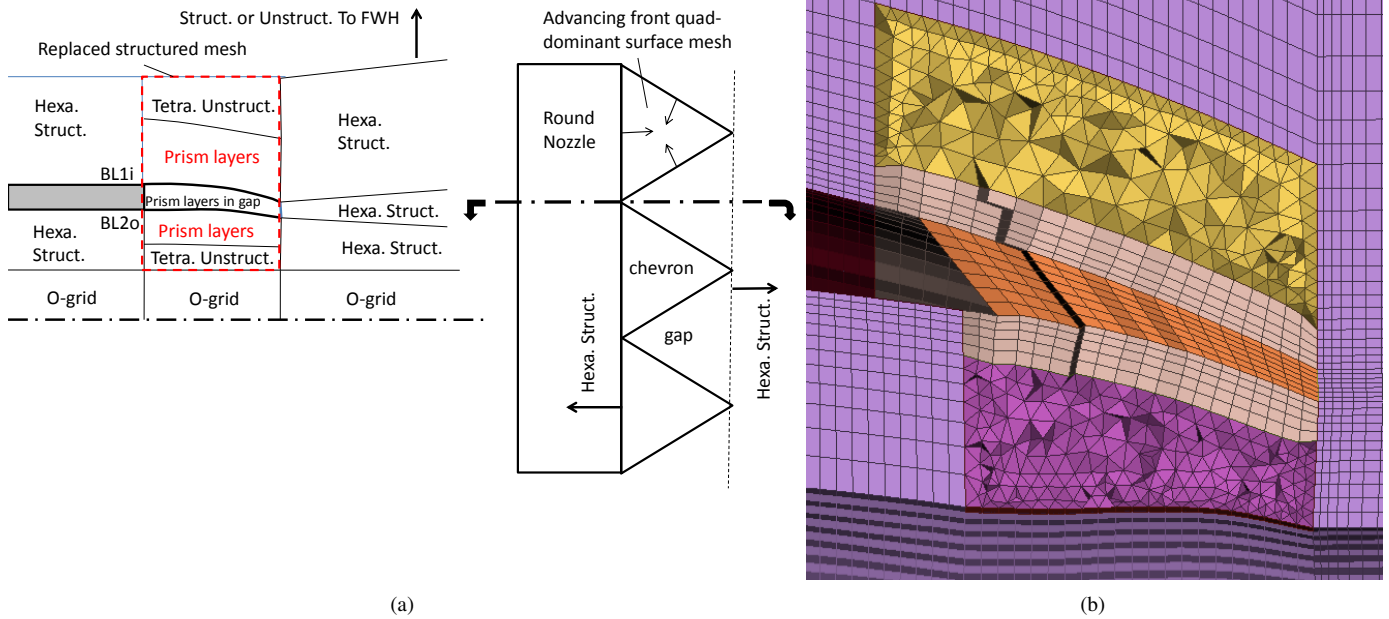
FIGURE 14. Localised unstructured meshing of a chevron nozzle, (a) topology, (b) example initial mesh cut-plane.
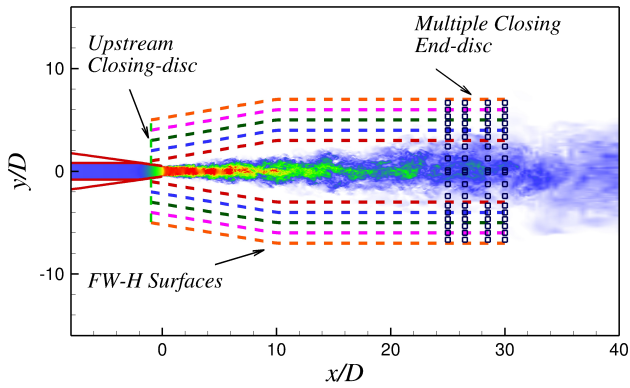
FIGURE 15. Multiple FW-H surfaces with upstream and multiple downstream closing discs.

TABLE 3. Operating conditions of the hot, cold and cold jet with flight stream. Subscripts j and ∞ refer to jet at the nozzle exit and far-field, respectively. U_j = jet exit velocity, $M_j = U_j/a_j$, a_j = sound velocity at nozzle exit, $M_a = U_j/a_\infty$, $M_\infty = U_\infty/a_\infty$, $TR = T_j/T_\infty$, T = temperature, $Re_D = \rho_j U_j D/\mu_j$ is Reynolds number based on D = jet diameter and μ_j =dynamic viscosity. J_1 =Hot Jet, J_2 =Cold Jet and J_3 =Cold Jet with Flight Stream.

	U_j	M_j	M_a	M_∞	TR	Re_D
J_1	297.7 (m/sec)	0.55	0.875	0.0	2.7	4×10^5
J_2	297.7 (m/sec)	0.875	0.875	0.0	1.0	2×10^5
J_3	297.7 (m/sec)	0.875	0.875	0.3	1.0	2×10^5

the hydrodynamic noise.

We have tested all these ideas to reveal an effective framework to use the FW-H method. To address the issue of the FW-H surface placement with respect to the jet, we have considered multiple FW-H surfaces at increasing distance from the jet centreline as shown in Figure 15. Three different jets are tested with these FW-H surfaces and their running parameters are defined in Table 3. In this case no closing disc at the upstream and downstream end of the FW-H surface is considered. The underlying flow grid determines the acoustic frequency resolution range of the FW-H surfaces. The upper limit of the Strouhal number resolved by the grid is given as $St_{max} = \frac{D/\Delta r}{8M_a}$ [55]. The grids for

the jet simulation are designed in such a way that just outside the active flow region, resolution decreases quickly. However, to place the FW-H surface away from the jet requires a higher grid resolution in the near acoustic field. The Strouhal number limits along the FW-H surfaces considered here for the three jets are given in Table 4.

The overall sound pressure level (OASPL) distribution at $100D$ and SPL spectra for three jets are given in Fig. 16, for various FW-H surfaces without closing discs. The angles for the OASPL are measured from the direction of the flow. Both OASPL and SPL spectra show that surfaces close to the jet generate spurious noise. As the FW-H surfaces are moved away from

TABLE 4. Radial grid spacing and Strouhal number limits along the four FW-H surfaces.

x/D		0	5	10	20	30
	FW-H 1	53	31	20	51	53
$D/\Delta r$	FW-H 2	22	17	14	25	27
	FW-H 3	14	11	10	16	17
	FW-H 4	9	8	7	12	12
	FW-H 1	7.7	4.5	2.9	7.3	7.7
St_{lim}	FW-H 2	3.2	2.5	1.9	3.6	3.8
	FW-H 3	1.9	1.6	1.4	2.2	2.5
	FW-H 4	1.3	1.2	1.1	1.7	1.7

the jet OASPL and SPL spectra collapsed to the measured values. At the higher and lower angles OASPL under-predict the measured values and under-prediction increases with the increasing distance of the FW-H surfaces from the jet. It shows the importance of open section of the FW-H surfaces at the upstream and downstream end, where most of the escaping noise is unaccounted for.

To account for the noise escaping from the upstream and downstream ends of the FW-H surface closing discs are introduced. The addition of upstream closing disc is a trivial exercise, because there are no significant flow structures upstream of the jet nozzle exit plane. The FW-H surface can be designed to follow the nozzle geometry closely for the acoustic waves moving upstream. However, use of the downstream closing discs is imperative to account for the escaping noise at low angles. As mentioned earlier passing vortical structures give spurious hydrodynamic noise from the closing disc. To suppress the effect of the hydrodynamic noise, there are eleven downstream closing discs in our tests. An averaging process on multiple closing discs can suppress the hydrodynamic noise. It has been suggested [55] that the disc averaging can suppress the hydrodynamic noise in the range of Strouhal numbers St;

$$\frac{U_c D}{2 U_j L} < St < \frac{U_c D}{2 U_j \Delta}, \qquad (3)$$

where, U_c is the local convective velocity at the closing discs, L is the distance between the first and the last disc and Δ is the distance between the individual discs. The averaging process can be performed in two different ways. One can consider each closing disc individually with the rest of the FW-H surface and can calculate the pressure far-field time series. In our case it gives 11 time series, which can be converted to Fourier space and averaged for each wave number and converted back to a single time series. We call this approach *far-field* averaging. In another approach, called *disc* averaging, each time step data on all the closing discs can be averaged in physical space and saved on a single disc. It can be used with the cylindrical part of the FW-H surface to calculate pressure far-field. There is also a possibility to use a partially closed disc rather than fully closed disc. In this case a disc starts from the cylindrical FW-H surface and stops near the outer edge of the jet shear layer. The location of the inner edge of the partially closed disc is arbitrary and flow dependent. In the current test cases we stopped the partially closed disc at a radial location, where u_{rms} is less than 10% of the maximum value at the given streamwise position.

Figure 17 shows the effect of the introduction of the closing discs on the far-field noise prediction on the jets tested here. The hot jet with surface 4 and closing discs give good results for OASPL and SPL spectra for the disc averaging as well as partially closing disc. In this case jet decay rate is higher and weak vortical structures pass through the closing disc. The averaging process aims to effectively cancel the effect of these structures. The cold jet and cold jet with a flight stream show that the disc averaging is unable to remove the hydrodynamic noise. The disc averaging for the jet with flight stream fails completely. The partial closing disc gives a better prediction for the two cold jets. However, the size of the partial closing disc is arbitrary, leading to two undesirable extremes of either a fully open or closed end disc. Hence, filtering may be a more reliable method as [57].

INDUSTRIALISATION OF JET LES

The complex flow fields produced by complex geometry jets require a robust process to become useful whilst reducing costs to acceptable levels. Figure 18 indicates an expert system based process for the industrial use of LES methods for jet aeroacoustics. The process based on flow classification (*A* for wake-type flow and *C* for high *Re* zones) is described in a similar way to LES of internal cooling and low-pressure turbine blades as [30]. The key process flows from top to bottom as indicated by the left hand side arrow. Each box (stage) has three rows, the first indicating inputs, the second, the process and the third, the output. In these, *US* and *ES* indicate input from the user or expert system respectively. Two key preliminary steps are the grid and boundary condition requirements defined by the flow classification. These can be used to estimate the cost-benefit ratio compared to alternatives such as experimental testing. If the simulation is feasible, mesh generation takes place and the case is run with additional computational control and data processing. Note, the use of carefully controlled mesh movement from a preliminary RANS-(N)LES or (N)LES mesh to a final mesh in the
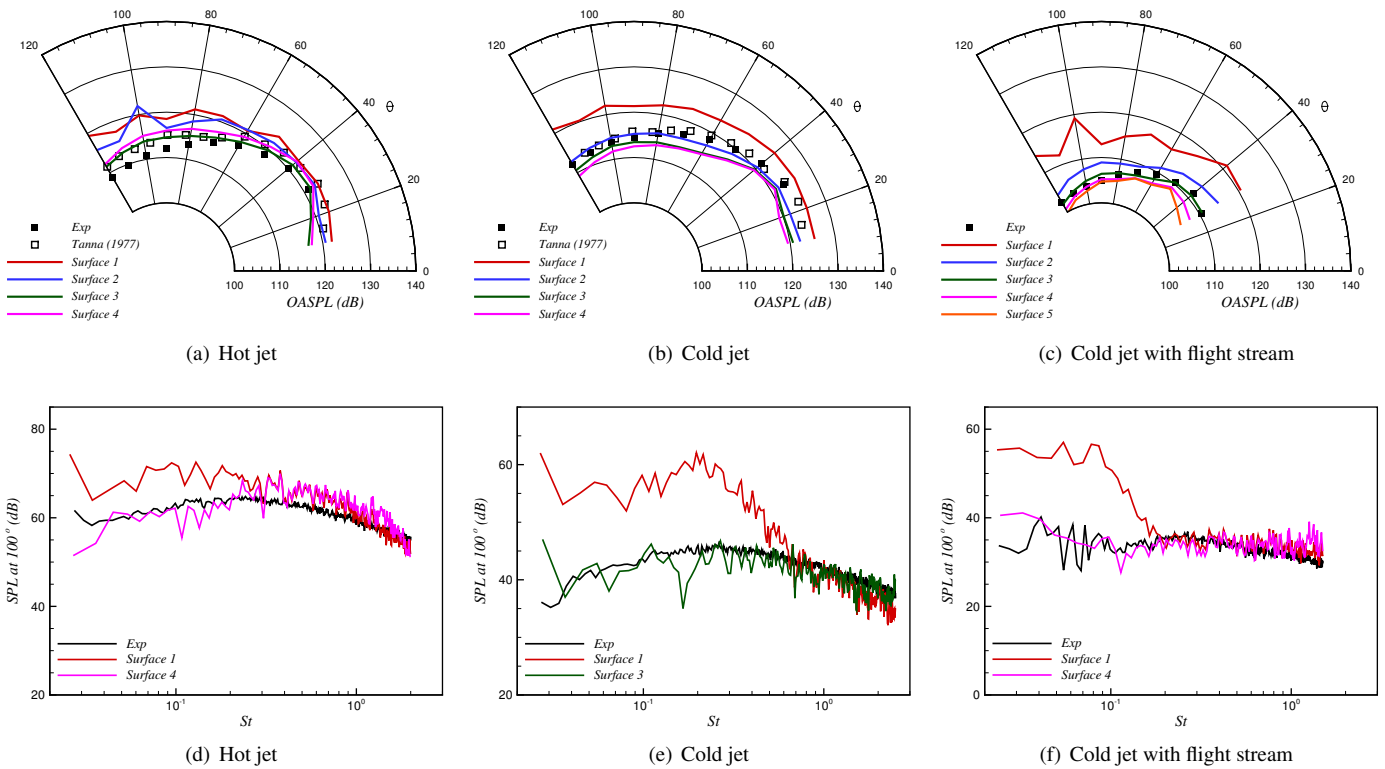
FIGURE 16.   OASPL and SPL spectra for the hot, cold and cold jet with flight stream without closing discs.

initial stages is particularly attractive for following shear layer evolution for chevron nozzles. The user is separated from modelling intricacies, best practices encompassed by the expert system. This will ensure consistency of (N)LES based simulations and accuracy of data. Data used and produced may also include upper and lower error bounds, confidence indicators, and known biases. In this way, when data is drawn from numerous sources, reliable predictive data can be produced with greater confidence.

In 2008, Bodony and Lele [2] stated the then current St achieved was in the range of $1.5 - 3$. Since then increases in computational power have led to significant progress towards higher and lower St due to increases in possible mesh size time series accumulation. Now, $0.1 < St < 5$ is readily achievable. Although computer peak performance has continued to grow at pace, a particularly concerning trend is that of the addition of large numbers of co-processor cards to boost peak performance on the worlds fastest super computers. As of June 2015, according to the top 500 list [58], four of the top 10 supercomputers now make use of graphics or other co-processors with an increase from 75 to 90 since November 2014 of the listed systems including some form of co-processors. The highly optimised code required to run on these architectures means only a small fraction of peak performance is often achieved. There is hence significant pressure to

develop or implement algorithms suited to these architectures to make the best use of available resources.

Quality Assurance

Ideally, as a predictive tool, (N)LES methods should be able to calculate accurate flow field and noise independent of any experimental data. However, RANS-(N)LES (or purely (N)LES), FW-H solvers and associated data analysis procedures need to be checked against benchmark test cases, to provide quality assurance and confidence for the whole process. Such a process requires experimental cases with the maximum possible detail, for example, nozzle geometry, upstream flow conditions inside the nozzle and jet entrainment conditions. There are few examples of measurements providing both flow and acoustic fields to test numerical results. Bridges and Wernet [59] have generated flow data for sub-sonic single stream jets including chevron nozzles. Tinney and Jordan [60] have provided the flow and sound data for coaxial jet and coaxial jet with chevrons. There is a shortage of joint flow and acoustic data for installed jets and jets with any significant flight stream. However, under these circumstances it can be useful to assess (N)LES based methods for simpler flows, without, for example, a flight stream and then apply the assessed (N)LES strategy to more industrially relevant flows. Hence, an
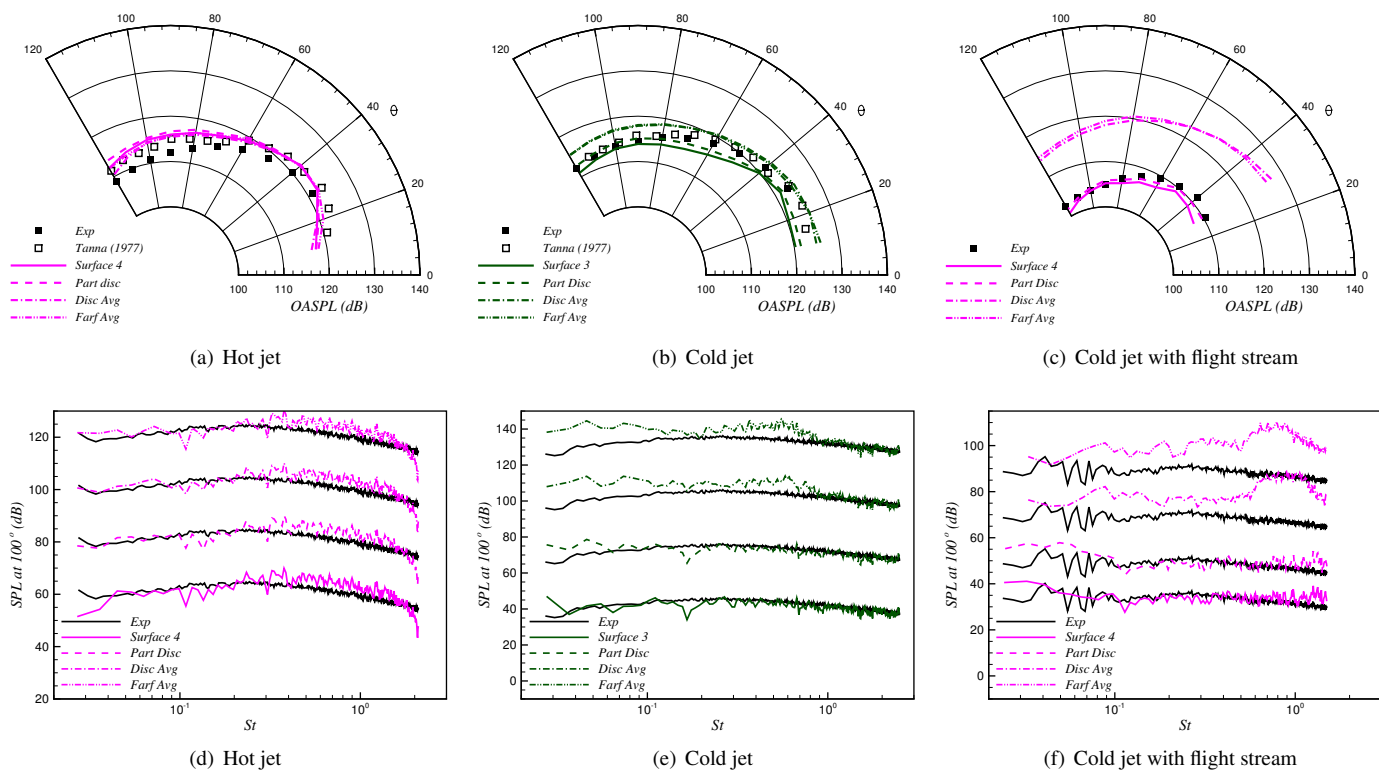
FIGURE 17. OASPL and SPL spectra for the hot, cold and cold jet with flight stream with closing discs.

indirect quality assurance procedure can be used. Ideally, spectral data for both the flow and acoustic fields along with 4th order space-time correlations and velocity-enthalpy fluctuations would enable a better understanding of acoustic source terms.

From an industry perspective, RANS-(N)LES and (N)LES is expected to show similar uncertainties with respect to predicting absolute jet and jet-flap interaction noise levels as known from large-scale tests. These can vary several dBs between facilities. However, the relative measurement accuracy of large-scale test facilities to a baseline configuration is in the order of 0.5EPNdB (Effective Perceived Noise dB). The target for the prediction accuracy of relative levels to a baseline achievable numerically over the next ten years should be 1EPNdB.

Cost

A typical rig test can cost several hundred thousand dollars. Clearly installed jets place considerably more cost relative to standard jet noise facilities. For business jets, the lower Reynolds numbers reduce the cost of RANS-(N)LES. This is seen as where RANS-(N)LES may first be used for jet aeroacoustics. Experimental campaigns often have relatively large time frames. RANS-(N)LES, when used in a controlled framework, has more predictable costs and is not purely limited to existing

noise test facilities but can be run on any available computational resource. Estimated typical RANS-(N)LES costs are provided in Tab. 5 however these will depend on commercial computing costs.

These are based on assuming a minimum meaningful Strouhal number of $St = 6$ for jet-flap interaction, $St = 10$ for jet noise of smaller engines and $St = 30$ for large engines and comparing this against the current cost of a $St = 3$ calculation. Future costs are also presented, assuming a run-time reduction factor of 5 to 20 by 2020 compared to 2014, due to more efficient use of new multi-core HPC architectures, local mesh refinements, more efficient alternatives to FW-H, Moores law and computing cost reduction.

Table 5 shows that the cost of (N)LES based predictions for jet-flap interaction and jet noise for small engines could be in the order or even lower than for large-scale tests and become an alternative for nozzle design verification. One would need at least 3 calculations, at the 3 certification points (approach, fly-over and sideline). Considering the in depth physics revealed by RANS-(N)LES, this presents a highly attractive cost-benefit ratio, especially as computational costs continue to fall.
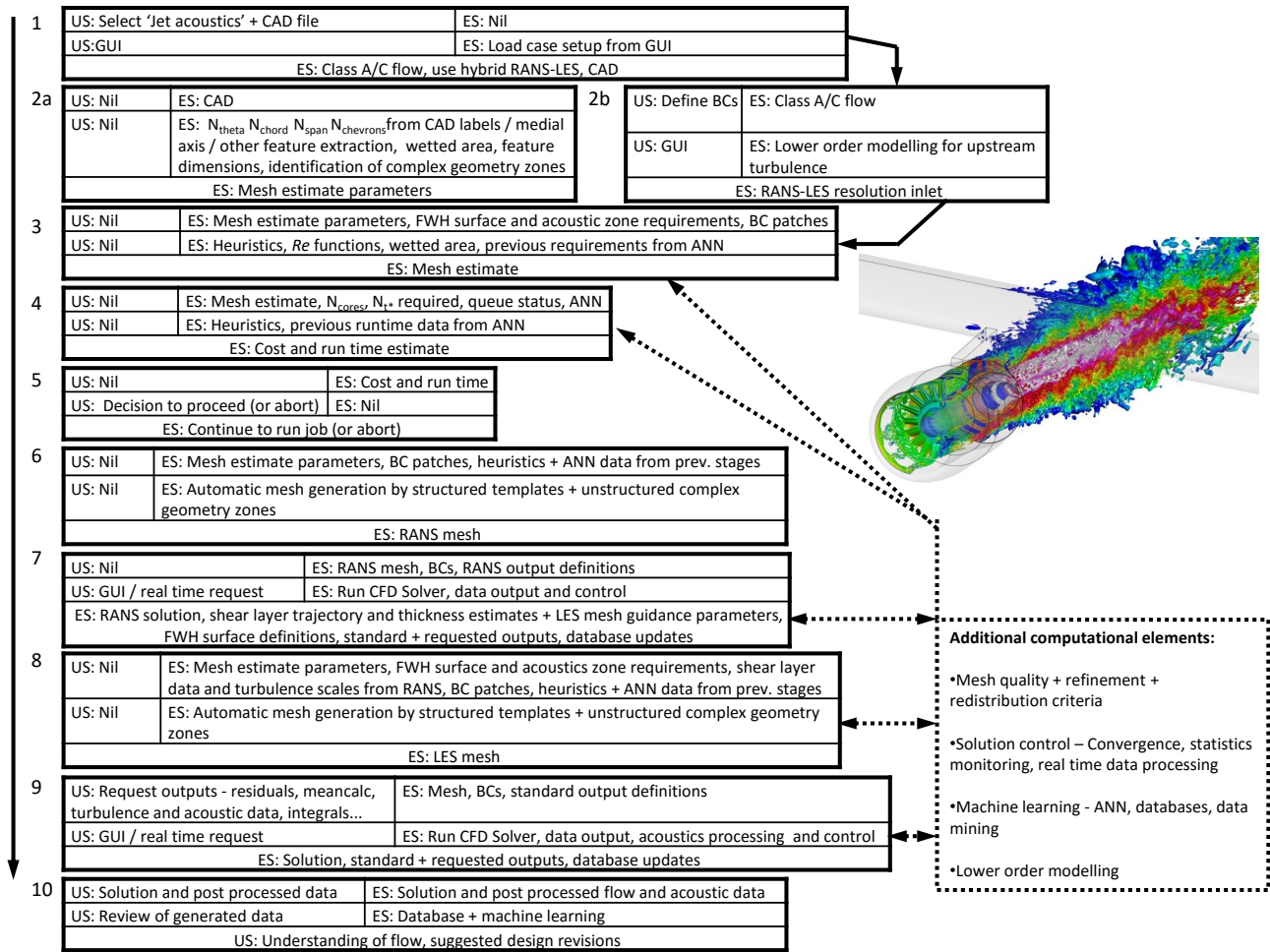
FIGURE 18. Example expert system based process for LES of complex jet aeroacoustics.

1	US: Select 'Jet acoustics' + CAD file	ES: Nil
	US: GUI	ES: Load case setup from GUI
	ES: Class A/C flow, use hybrid RANS-LES, CAD	

2a	US: Nil	ES: CAD
	US: Nil	ES: N_{theta} N_{chord} N_{span} $N_{chevrons}$ from CAD labels / medial axis / other feature extraction, wetted area, feature dimensions, identification of complex geometry zones
	ES: Mesh estimate parameters	

2b	US: Define BCs	ES: Class A/C flow
	US: GUI	ES: Lower order modelling for upstream turbulence
	ES: RANS-LES resolution inlet	

3	US: Nil	ES: Mesh estimate parameters, FWH surface and acoustic zone requirements, BC patches
	US: Nil	ES: Heuristics, Re functions, wetted area, previous requirements from ANN
	ES: Mesh estimate	

4	US: Nil	ES: Mesh estimate, N_{cores}, N_{t*} required, queue status, ANN
	US: Nil	ES: Heuristics, previous runtime data from ANN
	ES: Cost and run time estimate	

5	US: Nil	ES: Cost and run time
	US: Decision to proceed (or abort)	ES: Nil
	ES: Continue to run job (or abort)	

6	US: Nil	ES: Mesh estimate parameters, BC patches, heuristics + ANN data from prev. stages
	US: Nil	ES: Automatic mesh generation by structured templates + unstructured complex geometry zones
	ES: RANS mesh	

7	US: Nil	ES: RANS mesh, BCs, RANS output definitions
	US: GUI / real time request	ES: Run CFD Solver, data output and control
	ES: RANS solution, shear layer trajectory and thickness estimates + LES mesh guidance parameters, FWH surface definitions, standard + requested outputs, database updates	

8	US: Nil	ES: Mesh estimate parameters, FWH surface and acoustics zone requirements, shear layer data and turbulence scales from RANS, BC patches, heuristics + ANN data from prev. stages
	US: Nil	ES: Automatic mesh generation by structured templates + unstructured complex geometry zones
	ES: LES mesh	

9	US: Request outputs - residuals, meancalc, turbulence and acoustic data, integrals...	ES: Mesh, BCs, standard output definitions
	US: GUI / real time request	ES: Run CFD Solver, data output, acoustics processing and control
	ES: Solution, standard + requested outputs, database updates	

10	US: Solution and post processed data	ES: Solution and post processed flow and acoustic data
	US: Review of generated data	ES: Database + machine learning
	US: Understanding of flow, suggested design revisions	

Additional computational elements:

- Mesh quality + refinement + redistribution criteria
- Solution control – Convergence, statistics monitoring, real time data processing
- Machine learning - ANN, databases, data mining
- Lower order modelling

TABLE 5. Current and future costs of jet mixing and jet-flap interaction noise RANS-(N)LES computations.

St (Jet mixing noise)	Current cost ($)	Future 2020 cost ($)
3	35,000	1,800-7,000
10	1,300,000	65,000-260,000
30	35,000,000	1,800,000-7,000,000

St (Jet-flap interaction noise)	Current cost ($)	Future 2020 cost ($)
3	60,000	3,000-12,000
6	500,000	25,000-100,000

applicable filter definition are required. Realistic inflow or coupled system modelling may provide additional accuracy however at this time are considered secondary effects. Systematic procedures for FWH surface placement and end disc filtering mitigate potential difficulties and risks, particularly for installed jets and those with a flight stream. Hence, we see the industrial application of RANS-(N)LES for small scale industrial jets and installed jets as a viable tool in a foreseeable future time frame. Careful quality assurance and improved data at the spectral level for both the flow field and acoustics is needed with 4th order correlation data.

CONCLUSIONS

Strategies and numerical methods and processes have been shown for jet noise predictions. Their reliability has been demonstrated. Synergistic numerics, mesh, turbulence modelling and

NOMENCLATURE

Re	Reynolds number
U	Velocity, m/s
$\Delta x, y, z^+$	Grid spacings in wall units
x	Coordinate direction
ω	Vorticity, $1/s$
d	Wall distance
k	Turbulent kinetic energy
i	Variable index
ε	Turbulence dissipation rate

REFERENCES

[1] ACARE, 2001. European Aeronautics: A Vision for 2020. Tech. rep., Belgium.

[2] Bodony, D. J., and Lele, S. K., 2008. "Current Status of Jet Noise Predictions Using Large-Eddy Simulation". *AIAA Journal, 46*(2), feb, pp. 364–380.

[3] Bailly, C., and Juve, D., 2000. "Numerical solution of acoustic propagation problem using linearised Euler equations". *AIAA Journal, 38*(1), pp. 22–29.

[4] Bogey, C., and Bailly, C., 2010. "Influence of nozzle-exit boundary-layer conditions on the flow and acoustic fields on initially laminar jets". *J. Fluid Mech., 663*, pp. 507–538.

[5] Ffowcs Williams, J. E., and Hawkings, D. L., 1969. "Sound Generation by Turbulence and Surfaces in Arbitrary Motion". *Phil. Trans R. Soc. A, 264*, pp. 321–342.

[6] Pérez Arroyo, C., Daviller, G., Puigt, G., and Airiau, C., 2015. "Modal structure of a supersonic under-expanded jet". In 22ème Congrès Français de Mécanique, pp. 1–14.

[7] Pérez Arroyo, C., Puigt, G., and Boussuge, J.-F., 2016. "Large Eddy Simulation of Shock-Cell Noise From a Dual Stream Jet". In 22nd AIAA/CEAS Aeroacoustics Conference, Aeroacoustics Conferences, AIAA, pp. 1–20.

[8] Pérez Arroyo, C., Daviller, G., Puigt, G., and Airiau, C., 2015. "Hydrodynamic - Acoustic Filtering of a Supersonic Under-expanded Jet". In ERCOFTAC workshop Direct and Large- Eddy Simulation 10, pp. 1–6.

[9] Gefen, L., Pérez Arroyo, C., Camussi, R., Puigt, G., and Airiau, C., 2016. "Broadband Shock-cell Noise Signature Identification Using a Wavelet-based Method". In 22nd AIAA/CEAS Aeroacoustics Conference.

[10] Granados-Ortiz, F.-J., Lai, C.-H., Pérez Arroyo, C., Puigt, G., and Airiau, C., 2016. "Uncertainty Quantification and Sensitivity Analysis Applied to an Under-expanded Single Jet". In 46th AIAA Fluid Dynamics Conference, pp. 1–25.

[11] Gand, F., 2016. "Investigation of turbulence development in incompressible jets with zonal detached eddy simulation (ZDES) and synthetic turbulent inflow". *International Journal of Heat and Fluid Flow, In press*, pp. 1–13.

[12] Shur, M. L., Spalart, P. R., Strelets, M. K., and Travin, A. K., 2015. "An Enhanced Version of DES with Rapid Transition from RANS to LES in Separated Flows". *Flow, Turbulence and Combustion, 95*(1), pp. 709–737.

[13] Brunet, V., 2012. "Random Flow Generation Technique for Civil Aircraft Jet Simulations with the ZDES Approach". *Progress in Hybrid RANS-LES Modelling, 117*, pp. 193–204.

[14] Bres, G. A., Jaunet, V., Le Rallic, M., Jordan, P., Colonius, T., and Lele, S. K., 2015. "Large eddy simulation for jet noise : the importance of getting the boundary layer right". In 21st AIAA/CEAS Aeroacoustics Conference, AIAA, pp. 1–15.

[15] Cetin, M. O., Pauz, V., Meinke, M., and Schröder, W., 2016. "Computational analysis of nozzle geometry variations for subsonic turbulent jets". *Computers and Fluids, 136*, pp. 467–484.

[16] Verrière, J., Gand, F., and Deck, S., 2016. "Zonal Detached-Eddy Simulations of a Dual-Stream Jet". *AIAA Journal, 54*(10), pp. 3176–3190.

[17] Tyacke, J. C., Mahak, M., and Tucker, P. G., 2016. "Large-Scale Multifidelity, Multiphysics, Hybrid Reynolds-Averaged NavierStokes/Large-Eddy Simulation of an Installed Aeroengine". *Journal of Propulsion and Power*, pp. 1–12.

[18] Vogel, P., Bin, J., and Sinha, N., 2016. "LES predictions of jet noise for a pylon-mounted dual stream nozzle and jet surface interactions". In ASME Turbo Expo 2016, ASME, pp. 1–12.

[19] Rahier, G., Huet, M., and Prieur, J., 2015. "Additional terms for the use of Ffowcs Williams and Hawkings surface integrals in turbulent flows". *Computers and Fluids, 120*, pp. 158–172.

[20] Lyubimov, D. a., 2012. "Development and application of a high-resolution technique for jet flow computation using large eddy simulation". *High Temperature, 50*(3), pp. 420–436.

[21] Rosa, V., Self, R., Ilario, C., Naqavi, I., and Tucker, Paul, G., 2016. "Modelling Velocity Correlations with LES and RANS for Prediction of Noise from Isothermal and Hot Jets". In 22nd AIAA/CEAS Aeroacoustics Conference, AIAA, pp. 1–16.

[22] Karabasov, S. A., Afsar, M. Z., Hynes, T. P., Dowling, A. P., McMullan, W. A., Pokora, C. D., Page, G. J., and McGuirk, J. J., 2010. "Jet Noise : Acoustic Analogy Informed by Large Eddy Simulation". *AIAA Journal, 48*(7), pp. 1312–1325.

[23] Depuru Mohan, N. K., and Dowling, A. P., 2016. "Jet-

Noise-Prediction Model for Chevrons and Microjets". *AIAA Journal*, pp. 1–13.

[24] Towne, A., Jordan, P., Colonius, T., Jaunet, V., Schmidt, O. T., and Bres, G. A., 2016. "Trapped acoustic waves in the potential core of subsonic jets". In 22nd AIAA/CEAS Aeroacoustics Conference, AIAA/CEAS, pp. 1–18.

[25] Lapworth, B., 2004. "HYDRA CFD: A Framework for Collaborative CFD Development". In International Conference on Scientific and Engineering Computation.

[26] Naqvi, I. Z., Mahak, M., Wang, Z.-N., Tucker, P. G., and Strange, P., 2014. "An Assessment of Far-Field Noise Prediction for Subsonic Jets Using Large Eddy Simulation and Ffowcs Williams-Hawkings Method". In CFD Society of Canada 22nd Annual Conference, CFD Society of Canada.

[27] Wang, Z.-N., Naqvi, I. Z., Mahak, M., Tucker, P. G., Yuan, X., and Strange, P., 2014. "Far Field Noise Prediction for Subsonic Hot and Cold Jets Using Large-Eddy Simulation". In ASME Turbo Expo 2014: Turbine Technical Conference and Exposition, ASME, pp. 1–11.

[28] Xia, H., Tucker, P. G., and Eastwood, S., 2009. "Large-eddy simulations of chevron jet flows with noise predictions". *International Journal of Heat and Fluid Flow*, **30**(6), pp. 1067–1079.

[29] Tyacke, J., Tucker, P., Jefferson-Loveday, R., Rao Vadlamani, N., Watson, R., Naqvi, I., and Yang, X., 2013. "Large Eddy Simulation for Turbines: Methodologies, Cost and Future Outlooks". *Journal of Turbomachinery*, **136**(6), p. 061009.

[30] Tyacke, J. C., and Tucker, P. G., 2015. "Future Use of Large Eddy Simulation in Aero-engines". *J. Turbomach.*, **137**(8), pp. 081005–1–16.

[31] Spalart, P. R., and Allmaras, S. R., 1994. "A one-equation turbulence model for aerodynamic flows". *La Recherche Aérospatiale*, **1**(1), pp. 5–21.

[32] Tucker, P. G., 2003. "Differential equation-based wall distance computation for DES and RANS". *Journal of computational physics*, **190**(1), pp. 229–248.

[33] Smagorinsky, J., 1963. "General circulation experiments with the primitive equations. I. The basic experiment". *Monthly Weather Review*, **91**(3), pp. 99–165.

[34] Watson, R., Tucker, P. G., Wang, Z.-N., and Yuan, X., 2015. "Towards robust unstructured turbomachinery large eddy simulation". *Computers and Fluids*, **118**, pp. 245–254.

[35] Jameson, A., 2007. "Formulation of Kinetic Energy Preserving Conservative Schemes for Gas Dynamics and Direct Numerical Simulation of One-Dimensional Viscous Compressible Flow in a Shock Tube Using Entropy and Kinetic Energy Preserving Schemes". *Journal of Scientific Computing*, **34**(2), dec, pp. 188–208.

[36] Kawai, S., Shankar, S. K., and Lele, S. K., 2010. "Assessment of localized artificial diffusivity scheme for large-eddy simulation of compressible turbulent flows". *Journal*

of Computational Physics, **229**(5), pp. 1739–1762.

[37] Hill, D., and Pullin, D., 2004. "Hybrid tuned center-difference-WENO method for large eddy simulations in the presence of strong shocks". *Journal of Computational Physics*, **194**(2), pp. 435–450.

[38] Tam, C. K. W., 1998. "Advances in Numerical Boundary Conditions for Computational Aeroacoustics". *Journal of Computational Acoustics*, **6**(4), pp. 377–402.

[39] Bogey, C., and Bailly, C., 2002. "Three-dimensional non-reflective boundary conditions for acoustic simulations: Far field formulation and validation test cases". *Acta Acustica united with Acustica*, **88**(October), pp. 463–471.

[40] Poinsot, T. J., and K, L. S., 1992. "Boundary conditions for direct simulations of compressible viscous flows". *Journal of Computational Physics*, **101**(1), apr, pp. 104–129.

[41] Bogey, C., Marsden, O., and Bailly, C., 2012. "Influence of initial turbulence level on the flow and sound fields of a subsonic jet at a diameter-based Reynolds number of 10(5)". *Journal of Fluid Mechanics*, **701**(5), pp. 352–385.

[42] Uzun, A., and Hussaini, M. Y., 2012. "Some Issues in Large-Eddy Simulations for Chevron Nozzle Jet Flows". *Journal of Propulsion and Power*, **28**(2), mar, pp. 246–258.

[43] Birch, S. F., 2006. "A Review of Axisymmetric Jet Flow Data for Noise Applications". *12th AIAA/CEAS Aeroacoustics Conference (27th AIAA Aeroacoustics Conference)*.

[44] Batten, P., Goldberg, U., and Chakravarthy, S., 2004. "Interfacing Statistical Turbulence Closures with Large-Eddy Simulation". *AIAA Journal*, **42**(3), pp. 485–492.

[45] Keating, A., Piomelli, U., Balaras, E., and Kaltenbach, H.-J., 2004. "A priori and a posteriori tests of inflow conditions for large-eddy simulation". *Physics of Fluids*, **16**(12), pp. 4696–4712.

[46] Perret, L., Delville, J., Manceau, R., and Bonnet, J.-P., 2008. "Turbulent inflow conditions for large-eddy simulation based on low-order empirical model". *Physics of Fluids*, **20**(7), pp. 075107–1–17.

[47] Laraufie, R., Deck, S., and Sagaut, P., 2011. "A dynamic forcing method for unsteady turbulent inflow conditions". *Journal of Computational Physics*, **230**(23), sep, pp. 8647–8663.

[48] Lund, T. S., Wu, X., and Squires, K. D., 1998. "Generation of turbulent inflow data for spatially-developing boundary layer simulations". *Journal of Computational Physics*, **140**(2), pp. 233–258.

[49] Tucker, P., Coupland, J., Eastwood, S., Liu, Y., Jefferson-Loveday, R., and Hassan, O., 2006. "Contrasting Code Performances for Computational Aeroacoustics of Jets". *12th AIAA/CEAS Aeroacoustics Conference (27th AIAA Aeroacoustics Conference)*(October 2015).

[50] Mendez, S., Shoeybi, M., Sharma, A., Ham, F. E., Lele, S. K., and Moin, P., 2012. "Large-Eddy Simulations of Perfectly Expanded Supersonic Jets Using an Unstructured

Solver". *AIAA Journal, 50*(5), pp. 1103–1118.

[51] Shur, M. L., Spalart, P. R., and Strelets, M. K., 2005. "Noise prediction for increasingly complex jets. Part I : Methods and tests". *International Journal of Aeroacoustics, 4*(3-4), pp. 213–246.

[52] Bres, G. A., Nichols, J. W., Lele, S. K., and Ham, F. E., 2012. "Towards Best Practices for Jet Noise Predictions with Unstructured Large Eddy Simulations". In 42nd AIAA Fluid Dynamics Conference and Exhibit, AIAA, pp. 1–21.

[53] Brès, G. A., Khalighi, Y., Ham, F., and Lele, S. K., 2011. "Unstructured large eddy simulation technology for aeroacoustics of complex jet flows". In Inter-noise 2011, pp. 1–10.

[54] Brown, C., and Bridges, J., 2006. "Acoustic Efficiency of Azimuthal Modes in Jet Noise Using Chevron Nozzles". In 12th AIAA/CEAS Aeroacoustics Conference (27th AIAA Aeroacoustics Conference), pp. 1–14.

[55] Mendez, S., Shoeybi, M., Lele, S. K., and Moin, P., 2013. "On the use of the Ffowcs Williams-Hawkings equation to predict far-field jet noise from large-eddy simulations". *International Journal of Aeroacoustics, 12*(1+2), pp. 1–20.

[56] Mendez, S., Shoeybi, M., Sharma, A., Lele, S. K., and Moin, P., 2009. "Post-processing of large-eddy simulations for jet noise predictions". In Center for Turbulence Research, Summer Program, pp. 17–31.

[57] Naqvi, I. Z., Wang, Z.-N., and Tucker, P. G., 2016. "Far-field noise prediction for jets using Large-eddy simulation (LES) and Ffowcs Williams-Hawkings (FW-H) method". *International Journal of Aeroacoustics*, pp. 1–29.

[58] Meuer, H., Strohmaier, E., Dongarra, J., Simon, H., and Meuer, S., 2015. Top500 supercomputer list.

[59] Bridges, J., and Wernet, M. P., 2010. "Establishing Consensus Turbulence Statistics for Hot Subsonic Jets". In 16th AIAA/CEAS Aeroacoustics Conference, no. June, AIAA, pp. 1–41, Paper AIAA 2010–3751.

[60] Tinney, C. E., and Jordan, P., 2008. "The near pressure field of co-axial subsonic jets". *J. Fluid Mech., 611*, pp. 175–204.